JOURNAL OF GEOPHYSICAL RESEARCH, VOL. 100, NO. A10, PAGES 19,457–19,472, OCTOBER 1, 1995

Dispersive field line resonances on auroral field lines

A. Streltsov and W. Lotko

Thayer School of Engineering, Dartmouth College, Hanover, New Hampshire

Abstract. The formation of dispersive Alfvén resonance layers is investigated using a three-dimensional, two-fluid, magnetically incompressible model, including electron inertia and finite pressure. The equations are solved in "box" geometry with uniform magnetic field bounded by perfectly conducting ionospheres. Field line resonance (FLR) is stimulated within a density boundary layer with gradient transverse to ambient **B**; a parallel gradient in the Alfvén speed is also included. Numerical results show that the resonance amplitude is largest on the magnetic shell with eigenfrequency matching the frequency of the surface wave propagating on the density boundary layer. Efficient coupling between the resonant Alfvén wave and surface wave produces a relatively narrow FLR spectrum, even when the driver is broadbanded. Effective coupling to the external driver occurs only for long-wavelength azimuthal modes. It is shown that the parallel inhomogeneity limits radiation of dispersive Alfvén waves by the FLR. The results provide new insights into low-altitude satellite observations of auroral electromagnetic fields and the formation of discrete auroral arcs.

1. Introduction

It is becoming increasingly clear from theory and observations that two generic classes of auroral phenomena are often correlated. These include (1) transverse structure in electric and magnetic fields at spatial scales ranging from 1-10 km (referenced to the ionospheric height), including auroral arcs but not limited to luminous structures, with variations in time on the order of a few tens of seconds or greater, and (2) micropulsation phenomena associated with dispersive Alfvén waves leading to field line resonance (FLR) layers with a north-south extent of a few tens of kilometers or less in the ionosphere. Because field line resonance is a global feature of an auroral flux tube, understanding the nature of this correlation and the physical processes controlling its behavior promises a potentially powerful diagnostic for identifying the magnetospheric signatures of auroral arcs and associated low-altitude electromagnetic fields. The modeling effort described here represents a basic step in making this connection more quantitative.

Large-amplitude electromagnetic fluctuations are routinely observed on satellite auroral overpasses and usually are correlated with intense field-aligned electron fluxes [*Redsun et al.*, 1985] and sometimes auroral arcs [*Kletzing et al.*, 1983]. The interpretation of these fluctuations has been somewhat ambiguous, however, owing to difficulties in sorting out the spatiotemporal properties of long-period fluctuations on an orbiting platform. Both electrostatic [*Mozer et al.*, 1977; *Mozer*, 1980; *Burke et al.*, 1982] and Alfvénic [*Gurnett et al.*, 1984; *Chmyrev et al.*, 1988; *Dubinin et al.*, 1988] structures have been inferred. The spectral properties of electric and magnetic time series during some events [*Gurnett et al.*, 1984; *Weimer et al.*, 1985] show that the lowest-frequency fields, after accounting for effects of field-aligned potential drops, behave as Doppler-shifted, large-scale (100 km or greater), electrostatic or quasi-static fluctuations, whereas the properties of the higher-frequency components, corresponding to kilometer-scale structure, are in reasonable agreement with an Alfvén wave interpretation. A similar scale dependence has also been noted in the DE 2 [*Ishii et al.*, 1992] and Viking [*Block and Falthammar*, 1990] data sets, as well as in rocket experiments [*Boehm et al.*, 1990; *Knudsen et al.*, 1992].

However, low-frequency fields observed in the auroral zone do not always separate themselves into large-scale electrostatic structures and small-scale Alfvénic fluctuations. Ground-based observations show clear evidence for large-scale standing Alfvén waves, which may appear quasi-static in the rapidly moving reference frame of a polar orbiting satellite, whereas some small-scale disturbances are thought to be electrostatic, especially when their impedance characteristics differ significantly from those of a travelling Alfvén wave (ratio of transverse electromagnetic components **E**/**B** equal to the local Alfvén speed). It may be important that some small-scale Alfvénic fluctuations observed on polar-orbiting satellites are standing waves [*Dubinin et al.*, 1990], for which the respective nodes in the electric and magnetic fields are $\pi/2$ out of phase in time and are located at different positions along a field line. This fact may explain why the observed ratio, **E**/**B**, is sometimes much

Paper number 95JA01553.
0148-0227/95/95JA-01553$05.00

larger than the local Alfvén speed for some long-period Alfvénic signals mistakenly identified as electrostatic.

Ground-based observations provide direct evidence for a relationship between auroral luminosity variations, micropulsation phenomena, and standing Alfvén waves, although the usually low spatial resolution of the measurements does not allow direct comparison with the smaller-scale features deduced from polar orbiting satellites. Experiments using the EISCAT radars [*Haerendel et al.*, 1993] show time variations in auroral arcs associated with energy buildup, energy release, and oscillatory motion of the arc positions with periods in the Pc 5 range (several minutes). Correlations of signals in the 1-2 mHz range from ground magnetometers and meridian scanning photometers [*Xu et al.*, 1993] have shown that the energy of precipitating electrons in a relatively narrow, quiet time inverted-V structure is modulated at the frequency of a colocated FLR. Substorm related arcs, observed during both the preonset and recovery phases, also exhibit modulations in intensity at the frequencies of colocated FLRs in the Pc 5 range [*Samson et al.*, 1992; *Xu et al.*, 1993]. There is even evidence that FLRs may modulate electron precipitation in a widely separated auroral arc [*Samson et al.*, 1992]. In some cases the observed FLRs are barely resolvable in the range gates of the HF radar (resolution of 40 km), suggesting that the equatorial projection may be as small as a few plasma sheet ion Larmor radii [*Walker et al.*, 1992].

The approach taken here for modeling these phenomena is based on numerical solutions of the equations of two-fluid magnetohydrodynamics (MHD). Two-fluid MHD may be regarded as a minimal theoretical framework because the observed spatial scales, when mapped outward along an auroral flux tube, approach the electron inertial length in the lower magnetosphere and the ion/ion acoustic gyroradius in the equatorial magnetosphere; in addition, the observed temporal variations are comparable to (or greater than) the transit time of an Alfvén wave propagating between the equatorial magnetosphere and the ionosphere so that coupling between the magnetosphere and ionosphere is expected to be an important factor in the structural and dynamical properties of the fields. Various wave-particle interactions [*Temerin et al.*, 1986; *McFadden et al.*, 1987; *Li and Temerin*, 1993; *Allen*, 1993] are also important in the phenomenology but will not be pursued here.

Our numerical approach expands upon some earlier analytical studies by *Hasegawa* [1976] and *Goertz* [1984] on the influence of dispersive effects on resonant Alfvén waves, associated parallel electric fields arising from the dispersion, and their relation to discrete auroral arcs (see also *Haerendel* [1983]). At least two sources of dispersion are relevant. Electron inertial effects dominate in the lower magnetosphere and ionosphere while thermal effects are important at higher altitudes [*Lysak and Carlson*, 1981]. For example, an Alfvénic structure with a radial extent of the order of the ion/ion acoustic gyroradius in the equatorial plane ($\sim$ 100 km) maps to a structure at 1 R_E altitude with a north-south extent on the order of the local electron inertia length ($\sim$ few km). FLRs also become dispersive at larger scales ($\sim$ 1000 km radial) when effects of magnetic curvature and finite plasma pressure are included [*Kouznetsov and Lotko*, 1994]. In this paper we concentrate only on the relatively small-scale dispersive effects arising from electron inertia and finite pressure because the associated dispersion lengths are comparable to the observed thickness of discrete auroral forms.

Two previous numerical studies have shown that the "classical" (one-fluid MHD) FLR eventually saturates by radiating dispersive Alfvén waves if its amplitude and width are not first limited by other effects, for example, ionospheric dissipation [*Newton et al.*, 1978] or nonlinear spectral transfer [*Rankin et al.*, 1993]. Both the kinetic [*Inhester*, 1987] and electron inertial [*Wei et al.*, 1994] regimes have been considered, but only for cases where the system is taken to be homogeneous along the ambient magnetic field. The parallel inhomogeneity causes the Alfvén wave dispersion to change sign, from negative in the low-altitude, inertial regime to positive in the high-altitude, kinetic regime. The perpendicular group velocity of a dispersive Alfvén wave also changes sign where the dispersion changes sign, which causes a radiated dispersive Alfvén wave to dwell near resonance much longer than in a medium without the parallel inhomogeneity. As shown here, this behavior, combined with wave reflection off the conducting ionospheres, significantly retards radiative losses by a FLR. As a consequence these losses may be much less effective in limiting the resonance than previously thought.

The numerical study by *Inhester* [1987] considers the formation of a dispersive FLR in a large-scale perpendicular gradient in the Alfvén speed, corresponding to the radial increase in the geomagnetic field strength. In this paper we consider (like *Wei et al.* [1994]) the excitation of a dispersive FLR in a relatively thin density boundary layer (thickness of approximately 1 R_E or less transverse) that may be superimposed on the larger-scale variation in Alfvén speed. *Hasegawa* [1976] has shown that an MHD surface wave propagating on the density boundary layer couples to an FLR residing within the layer. One consequence of this coupling, as shown here, is a tendency for a single mode resonance (including its harmonics) to be preferentially selected, even when the "external driver" is broadband in frequency. The observation of isolated density boundary layers in the near-Earth plasma sheet region is not well documented in the literature, although their existence has been emphasized by *McIlwain* [1980], and there is at least one definitive observation [*Hughes and Grard*, 1984] of isolated layers. We point out in the discussion section that plasma measurements on the AMPTE/IRM satellite also provide evidence for the existence of density boundary layers in the same region.

Finally, our numerical results show a tendency for the power in a dispersive FLR to be focused at low altitude near the location of the peak in the Alfvén speed. This result suggests that dispersive FLRs may serve as effec-

tive generators for the very small spatial scale and high-frequency (0.1-1 Hz) inertial Alfvén waves that become trapped at relatively low altitudes in the "ionospheric Alfvén resonator" [*Polyakov and Rapoport*, 1981]. This resonant cavity, resulting from wave refraction near the low-altitude maximum in the Alfvén speed, is not resolved in the computations described here. Our results therefore complement a number of other studies that focus on discrete modes in the Alfvén resonator [*Trakhtengertz and Feldstein*, 1991; *Lysak*, 1991] and various nonlinear effects leading to local instabilities of the resulting velocity/magnetic shear layers [*Seyler*, 1988, 1990; *Streltsov et al.*, 1990; *Chmyrev et al.*, 1992] that are important during auroral breakup.

2. Theory

2.1. Reduced Two-Fluid Model

The region spanned by nightside auroral flux tubes, extending from northern to southern ionospheres, will be modeled as a magnetized, collisionless, low-β plasma. For simplicity, the background magnetic field is taken to be uniform (so-called "box model"). The plasma is assumed to be initially free of bulk flows and electrical currents. The low-frequency electromagnetic perturbations considered here are characterized by (1) low sonic Mach number and (2) high aspect ratio (characteristic of a shear Alfvén wave), in which the scale size $L_\parallel$ of the perturbation along the background magnetic field is much larger than the perpendicular scale size $L_\perp$.

More specifically, the following hierarchy of small parameters ($\epsilon^2 \ll 1$) is used in the derivation [*Chmyrev et al.*, 1988] of the reduced two-fluid equations given below:

$$\epsilon^2 \sim \omega_{ci}^{-1}\partial/\partial t \sim v_{Ti}^2\omega_{ci}^{-2}\nabla_\perp^2 \sim (E_\perp/B_0 v_{Ti})^2 \sim (L_\perp/L_\parallel)^2.$$

Here ω_{ci} is the local ion gyrofrequency, v_{Ti} is the local ion thermal speed, and the subscripts $\perp$ and $\parallel$ denote vector components in the directions locally perpendicular and parallel to the ambient magnetic field. The reduced two-fluid equations include, in order of appearance, electron parallel momentum, electron mass continuity, current continuity combined with ion momentum, and ion energy:

$$m_e n\frac{dv_{\parallel e}}{dt} + enE_\parallel + \hat{\mathbf{b}}\cdot\nabla p_e = 0$$

$$\frac{dn}{dt} + \nabla\cdot nv_{\parallel e}\hat{\mathbf{b}} = 0$$

$$\nabla\cdot j_\parallel\hat{\mathbf{b}} + e\nabla\cdot\left[\frac{d}{dt}\left(en\mathbf{E}_\perp - \nabla_\perp p_i\right)/m_i\omega_{ci}^2\right] = 0$$

$$\frac{dp_i}{dt} = 0.$$

Subsidiary equations include

$$\mathbf{B} = \mathbf{B}_0 + \nabla A_\parallel \times \mathbf{B}_0/B_0$$

$$E_\parallel = -\hat{\mathbf{b}}\cdot\nabla\phi - \frac{1}{c}\frac{\partial A_\parallel}{\partial t}$$

$$v_{\parallel e} = \frac{c}{4\pi ne}\nabla_\perp^2 A_\parallel$$

$$p_e = nT_e.$$

The low-β of the plasma, together with the high aspect ratio of the fluctuations, simplifies the mathematical specification of the magnetically incompressible perturbations described by the model, as characterized by a scalar electric potential ϕ and a scalar flux function $A_\parallel$, corresponding to the single parallel component of the perturbed vector potential [*Kadomtsev*, 1965]. The total time derivative, $d/dt = \partial/\partial t + \mathbf{v}_E\cdot\nabla$, includes explicit time variation as well as convective variations with $\mathbf{v}_E = \mathbf{E}\times\mathbf{B}/B^2$. The quasi-neutral plasma density, n, and ion and electron pressures, $p_{i,e}$, include both background and perturbed parts. $\hat{\mathbf{b}}$ is a unit vector pointing in the local direction of the background $\mathbf{B}_0$ plus perturbed $\nabla A_\parallel\times\mathbf{B}_0/B_0$ magnetic field. Because the field-aligned current is carried primarily by the electrons, to a good approximation, $j_\parallel \approx -env_{\parallel e} = (c/4\pi)\nabla_\perp^2 A_\parallel$. Effects of ion polarization and gyroviscosity are included in the current continuity equation; to obtain the gyroviscous contribution given above, it is necessary to retain the gyroviscous stress tensor in the ion momentum equation [*Hazeltine and Meiss*, 1985]; an equivalent procedure involves averaging the ion Vlasov equation over gyrophase, retaining only first-order terms in the small parameter ϵ before computing moments [see *Chmyrev et al.*, 1988].

These equations will be solved in a slab geometry, in which the z direction is along the background magnetic field; the x direction points along the perpendicular gradient in background Alfvén speed (mapping to the ionospheric north-south direction); and the y direction completes the right-hand system (mapping to the ionospheric east-west direction).

The following dimensionless variables are introduced:

$$\omega_{ci}t \to t,\ (\omega_{ci}/c_s)r_\perp \to r_\perp,\ (\omega_{ci}/v_A)z \to z,$$

$$e\phi/T_{e0} \to \Phi,\ eA_\parallel v_A/cT_{e0} \to A,\ n/n_0 \to N = N_b + N_d,$$

$$p_i/n_0T_{e0} \to P_i = P_{ib} + P_{id},\ p_e/n_0T_{e0} \to P_e = P_{eb} + P_{ed}.$$

Subscripts b and d denote background and disturbed, respectively; the constants T_{e0}, n_0, ω_{ci}, c_s, and v_A are fixed values of electron temperature, density, ion cyclotron frequency, ion sound speed based on T_{e0}, and Alfvén speed, which are chosen at some particular point in the inhomogeneous system, for example, at the equatorial plane at a radial distance of 9 R_E.

For a flow-free and current-free unperturbed state, the electron parallel momentum equation requires $\partial_z P_{eb} = 0$. To simplify the analysis, the electron temperature T_e will be taken to be constant throughout the region of interest so that $P_e = (N_b + N_d)T_e$. An isothermal approximation for the electron fluid is reasonable at high altitude where the electron thermal speed exceeds the Alfvén speed. At lower altitudes the electrons would

probably be better modeled by some sort of adiabatic equation of state; however, the electron response is primarily inertial in the low-altitude region, so the particular choice of electron equation of state is of less importance in this region (see also section 2.3, below).

With this specification for the electron pressure, and in the limit of small amplitudes leading to a linear approximation, the reduced two-fluid equations take the form

$$N_b \frac{\partial}{\partial t} A - \delta \frac{\partial}{\partial t} \nabla_\perp^2 A = \frac{\partial}{\partial z} N_d + \frac{\partial N_b}{\partial x} \frac{\partial A}{\partial y} - N_b \frac{\partial}{\partial z} \Phi \quad (1)$$

$$\frac{\partial}{\partial t} N_d = -\frac{\partial}{\partial z} \nabla_\perp^2 A + \frac{\partial N_b}{\partial x} \frac{\partial \Phi}{\partial y} \quad (2)$$

$$\frac{\partial}{\partial t} (\nabla \cdot N_b \nabla_\perp \Phi) = -\frac{\partial}{\partial z} \nabla_\perp^2 A - \nabla \cdot \{P_{ib}, \nabla_\perp \Phi\} \quad (3)$$

$$\frac{\partial}{\partial t} P_{id} = \{P_{ib}, \Phi\}, \quad (4)$$

where $\{A, B\} = (\partial A/\partial x)(\partial B/\partial y) - (\partial A/\partial y)(\partial B/\partial x)$. The nondimensional parameter δ appearing in (1) is an important parameter of the model and can be expressed in terms of various ratios as

$$\delta = \frac{m_e}{m_i} \frac{2}{\beta_e} = \frac{v_A^2}{v_{Te}^2} = \frac{c^2}{\omega_{pe}^2 \rho_s^2}.$$

Here β_e is the electron β, and v_{Te} is the electron thermal speed. Because the disturbed part of the ion pressure does not appear in the right-hand sides of the linearized equations, the variable P_{id} is "enslaved," and (4) can be excluded from the main solution (it is shown here only for completeness).

Although the set (1)-(3) with harmonic time variation will be solved numerically for arbitrary density gradients, useful physical insights can be derived from simple linear dispersion characteristics when the density and pressure gradients are weak. When the background density and ion pressure vary linearly with x ($P_{ib} = 1 + \kappa_P x$ and $N_b = 1 + \kappa_N x$ with $\kappa_P, \kappa_N \ll k_\perp < 1$), the dispersion relation can be given as [*Chmyrev et al.*, 1988]

$$k_\perp^2 [k_z^2(\omega + \kappa_N k_y) - (\omega^2(1 + \delta k_\perp^2) + \kappa_N \omega k_y - k_z k_\perp^2)(\omega - \kappa_P k_y)] = 0.$$

Both incompressible surface waves ($k_\perp^2 = 0$) and dispersive drift–Alfvén waves (square bracket [...] = 0) are included. The dispersive Alfvén and drift waves decouple when $k_z \gg \kappa_N k_y, \kappa_P k_y$. The resulting (decoupled) dispersion relations are, for drift waves,

$$\omega = \frac{k_\perp^2 \kappa_P k_y - \kappa_N k_y}{1 + k_\perp^2},$$

and for Alfvén waves,

$$\omega^2 = k_z^2 \frac{1 + k_\perp^2}{1 + \delta k_\perp^2}.$$

The first and second terms in the numerator of the drift wave dispersion relation represent ion and electron drift terms, respectively. The term $\delta k_\perp^2$ in the denominator of the Alfvén wave dispersion relation is due to the finite electron inertia [*Goertz and Boswell*, 1979], which provides negative dispersion; the factor $k_\perp^2$ in the numerator is due to the finite electron temperature, which provides positive dispersion. When electron inertial effects dominate the Alfvén wave dispersion ($\delta > 1$), we refer to the wave as an "inertial" Alfvén wave; when finite thermal effects dominate the dispersion ($\delta < 1$), the wave is identified as a "kinetic" Alfvén wave because the form (though not necessarily the magnitude) of the dispersion is identical to that obtained from an ion kinetic treatment [*Hasegawa*, 1976].

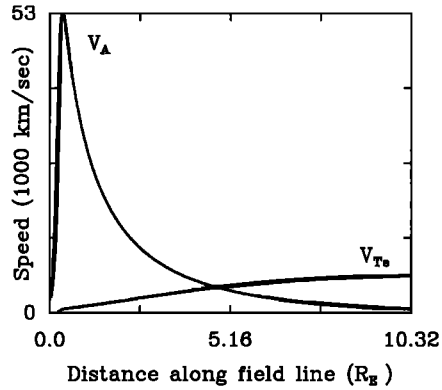

Figure 1. Alfvén and electron thermal speeds as functions of distance along a magnetic field line from the ionosphere ($0R_E$) to the equatorial plane ($10.32R_E$). The magnetic field line is traced from the equatorial plane at 9 R_E geocentric distance at 2400 MLT using the truncated *Tsyganenko* [1987] model with $K_p = 2^-, 2, 2^+$. The density model is based on $n = 2.25 \times 10^{18} e^{-29.4r} + Ar^{-3} + 0.6$ (similar to that of *Lysak and Carlson* [1981]) where r is geocentric distance measured in R_E, and A is chosen so that the density at $r = 2$ is equal to 25 cm^{-3}. The electron temperature at the equator has been set equal to 250 eV.

Both negative and positive dispersion are relevant for Alfvén waves propagating or standing between the two auroral ionospheres [*Lysak and Carlson*, 1981]. At low altitude, $\delta \gg 1$, whereas near the equatorial crossing point of the auroral field line, $\delta \ll 1$. The transition from inertial to kinetic regimes occurs approximately midway between the ionosphere and equatorial plane where $\delta = 1$ (or $v_A = v_{Te}$). Figure 1 shows a "typical" variation of the electron thermal speed versus distance along a nightside field line that crosses the equatorial plane at a radial distance of 9 R_E. In the dispersion transition region, at an altitude of about 4–6 R_E where the electron thermal and Alfvén speeds are comparable, the dispersive Alfvén wave also encounters electron Landau damping owing to its parallel electric field. Effects of Landau damping are not included in the reduced two-fluid model considered here.

In a homogeneous plasma the parallel electric field and Landau damping rate for a dispersive Alfvén wave are proportional to $k_\perp^2$ times the appropriate dispersion length squared, either the electron inertial length when $\delta > 1$ or the ion acoustic gyroradius when $\delta < 1$. Therefore electron Landau damping is negligible when

$k_\perp$ is sufficiently small. In an inhomogeneous plasma in which the Alfvén speed varies in the perpendicular direction, the effective $k_\perp$ (to the extent that one can discuss a local value of the wavenumber in an inhomogeneous plasma) approaches zero at points where the wave ceases to propagate in the perpendicular direction. This is precisely what occurs near a dispersion-limited field line resonance as discussed below (see also *Hasegawa* [1976]), so that the wave parallel electric field and electron Landau damping are expected to be weak in the immediate neighborhood of the resonance. How important Landau damping becomes away from field line resonance, or how quickly it becomes appreciable, is not known. One possibility is that the radiated dispersive Alfvén waves discussed later in the paper become strongly attenuated as they propagate away from the field line resonance layer (with an attendant increase in the effective perpendicular wave number). On the other hand, the fact that the dispersive Alfvén wave spends only a limited time in the transition/dissipation region (where $v_A \approx v_{Te}$) may significantly limit the net attenuation of the wave. When field line resonance is considered as an initial value problem, Landau damping, together with ionospheric Ohmic dissipation, may also limit the spatial width of the resonance and therefore the bandwidth of effective perpendicular wavenumbers. It is fair to say that the Landau damping of resonant, dispersive Alfvén waves in a strongly inhomogeneous plasma is not well understood, especially for the type of parallel inhomogeneity that arises on auroral field lines.

2.2. FLR Without Parallel Inhomogeneity

Field line resonance is possible when the Alfvén speed varies in the direction perpendicular to the background magnetic field [*Chen and Hasegawa*, 1974a; *Southwood*, 1974]. The resonance occurs at the location where the frequency of oscillation matches the eigenfrequency of a shear Alfvén wave standing along a magnetic shell between the two conducting ionospheres. In one-fluid MHD with background magnetic field in the z direction and Alfvén speed gradient in the x direction, E_x and B_y have a pole singularity at the resonant surface. This singularity is resolved when finite ion Larmor radius effects, finite electron pressure, or finite electron inertia, alone or in combination, are included [*Hasegawa*, 1976; *Goertz*, 1984]. However, the resolved wave amplitude still remains large near the resonance point. The resolved wave profile in the x–direction resembles the Airy function $Ai(x)$ with its oscillatory peak located near the resonant field line [*Hasegawa*, 1976]. To develop some physical insights into the numerical solutions of dispersive field line resonances discussed in the next section, we first consider a simple case when the plasma is inhomogeneous in the perpendicular direction but homogeneous in the parallel direction. Some qualitative features of the problem, including both types of inhomogeneity, are then discussed before considering the full numerical problem.

Suppose the plasma is homogeneous along the ambient magnetic field and let the ambient ion pressure and plasma density vary with x so that $N_b = N_b(x)$ and $P_b = P_b(x)$. Now seek solutions to the linear set (1)–(3) in the form of waves propagating in the x (radial) and y (azimuthal) directions but standing between two perfectly conducting ionospheres where $\Phi = 0$:

$$A(x,y,z,t) = A(x)\cos(k_z z)\cos(\omega t - k_y y)$$

$$\Phi(x,y,z,t) = \Phi(x)\sin(k_z z)\sin(\omega t - k_y y)$$

$$N_d(x,y,z,t) = N_d(x)\sin(k_z z)\sin(\omega t - k_y y).$$

Equations (1)–(3) can then be reduced to

$$N_d = \nabla \cdot N_b \nabla_\perp \Phi - \alpha\left(\frac{\partial P_{ib}}{\partial x}\nabla_\perp^2\Phi + \frac{\partial N_b}{\partial x}\Phi\right) \quad (5)$$

$$v_z A = \frac{\delta v_z^2 - 1}{N_b + \alpha\frac{\partial N_b}{\partial x}}\left(\nabla \cdot N_b\nabla_\perp\Phi - \alpha\frac{\partial P_{ib}}{\partial x}\nabla_\perp^2\Phi\right) + \Phi \quad (6)$$

$$\nabla_\perp^2\left(\Phi + \frac{\delta v_z^2 - 1}{N_b + \alpha\frac{\partial N_b}{\partial x}}\left(\nabla \cdot N_b\nabla_\perp\Phi - \alpha\frac{\partial P_{ib}}{\partial x}\nabla_\perp^2\Phi\right)\right) - v_z^2\nabla \cdot N_b\nabla_\perp\Phi = 0 \quad (7)$$

with $\nabla_\perp^2 = \partial_x^2 - k_y^2$, and

$$\nabla \cdot N_b\nabla_\perp = \frac{\partial}{\partial x}N_b\frac{\partial}{\partial x} - N_b k_y^2.$$

The notation $v_z = \omega/k_z$ and $\alpha = k_y/\omega$ has been introduced, and small terms resulting from the orderings $|\partial^2 P_{ib}/\partial x^2| \ll k_\perp^2$ and $|\partial^2 N_b/\partial x^2| \ll k_\perp^2$ have been neglected.

Equation (7) is similar to the fourth-order wave equations derived previously by *Hasegawa* [1976] and *Goertz* [1984]; the additional terms included here involve electron and ion drift waves associated with the inhomogeneities in N_b and P_{ib}. Once the background density and pressure are given, (7) can be solved numerically on any finite interval with appropriate boundary conditions.

When $k_y = 0$, the drift wave terms disappear, and (7) can be reduced to a second-order equation for the electric field ($E_x = -\partial_x\Phi$),

$$\frac{\partial}{\partial x}\left(\frac{1}{N_b}\frac{\partial}{\partial x}(N_b E_x)\right) + \frac{v_z^2 N_b - 1}{1 - \delta v_z^2}E_x = E_0. \quad (8)$$

E_0 is an integration constant related to the boundary condition on E_x far from the resonant point.

Equation (8), or a similar form, with $N_b(x) = 1 + \kappa_N x$ and κ_N small, has been studied extensively in relation to the mode conversion of an electromagnetic wave to a Langmuir wave [e.g., *Stix*, 1992]. As discussed by *Hasegawa* [1976] the mode conversion of a MHD surface wave to a kinetic Alfvén wave is analogous. It is well known that the solution can be expressed in terms of Airy functions.

A plot of the solution to (7) with $\delta = 0$, $k_y = 0$, and $v_z = 1$ for the perpendicular density and Alfvén speed profiles shown in Figure 2 is given in the upper

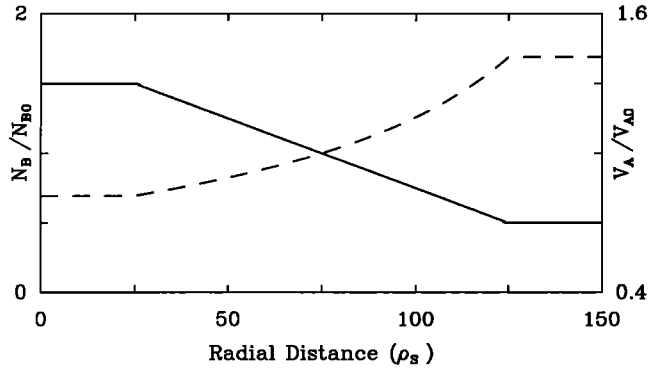

Figure 2. The profiles of the density (solid line) and Alfvén speed (dashed line) in the perpendicular (radial) direction. These profiles are used in all subsequent computations.

panel of Figure 3. This solution contains a large-scale variation in x, corresponding to the MHD surface wave, and a small-scale oscillation due to the kinetic Alfvén wave. The amplitude and wavelength of the small-scale oscillation varies with x in the region of the density gradient ($25 < x < 125$) where the pattern resembles an Airy function. The amplitude and wavelength of the oscillation are constant for $x < 25$ where the density and Alfvén speed are constant. The oscillation is evanescent to the right of the peak oscillation or resonance.

In order to separate the oscillations at different scale lengths, the Fourier spectrum of the solution shown in the upper panel of Figure 3 is filtered. The middle panel in Figure 3 shows the Fourier transform of the solution (thin curve) and the low-pass filtering function (thick curve). The bottom panel in Figure 3 shows the solution after convolution with the filter (thick curve), as well as its residual (thin curve), obtained as the difference between the full solution and its filtered part. As expected from the linear dispersion relation, the kinetic Alfvén wave propagates in the higher-density (lower Alfvén speed) region to the left of the resonance point where $\omega/k_{\|} > v_A$. The wave amplitude increases as the "resonance" is approached from the left, while the effective perpendicular wavenumber k_x decreases. Near the critical point where the parallel phase speed matches the local Alfvén speed (at $x = 75\rho_i$), the effective wavenumber becomes zero. To the right of this point the wave is evanescent. Had we considered a case where $\delta > 1$ rather than $\delta = 0$, implying that electron inertia (and associated negative dispersion) dominates the Alfvén wave dispersion, we would have found a similar pattern, but one mirrored left to right about the resonance point.

For $k_y = 0$ the surface wave satisfies a type of jump condition in x. At points outside the background density ramp shown in Figure 2, the electric field described by (8) becomes

$$E_{x_{1,2}} = \frac{1 - \delta v_z^2}{N_{1,2} v_z^2 - 1} E_0.$$

Here, $E_{x_{1,2}}$ represents the values of the electric field in the homogeneous regions where the background density takes on the constant values $N_{1,2}$. To the left of the density ramp, $N_1 v_z^2 > 1$ so $E_{x_1} > 0$ whereas to the right, $N_2 v_z^2 < 1$ so $E_{x_2} < 0$. The fact that E_x is constant in the homogeneous regions is a consequence of setting $k_y = 0$. When $k_y \neq 0$, the surface wave electric field E_x varies as $\pm \exp(-k_y|x - x_r|)$ in the homogeneous regions where x_r is the location of the resonant field line.

The efficiency of resonant coupling between the surface wave and kinetic Alfvén wave is illustrated in Figure 4 for $k_y = 0$ and for various values of the parallel phase speed v_z and the gradient scale length of the background density ramp. The figure shows the peak amplitude of E_x calculated from (7) and its location in the density ramp of Figure 2. Each curve represents a family of solutions obtained by varying the parallel phase speed over the range $0.85 < v_z < 1.30$. (v_z is the parallel phase speed normalized to the Alfvén speed at the center of the ramp at $x = 75\rho_i$.) The extreme values are near the minimum and maximum values, respectively, in the Alfvén speed shown in Figure 2. The solid, short-dashed, and long-dashed curves correspond to an over-

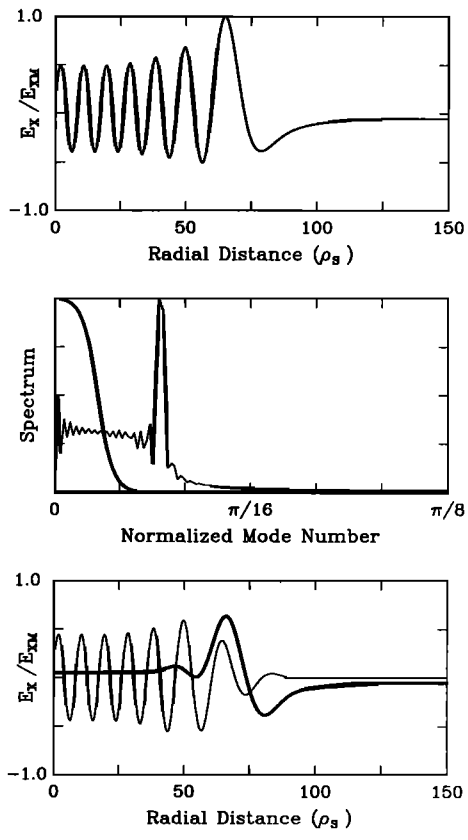

Figure 3. (upper panel): The perpendicular electric field E_x, normalized to its maximum value E_{xm}, corresponding to the resonance solution of (7) with $k_y = 0$ and $v_z = 1$ for the density profile shown in Figure 2. (middle panel): The spectrum of the solution (thin curve) and filtering function (thick curve). (lower panel): The low-frequency (thick curve) and high-frequency (thin curve) portions of the solution. The low-frequency portion is associated with the surface wave; the high-frequency part corresponds to the kinetic Alfvén wave.

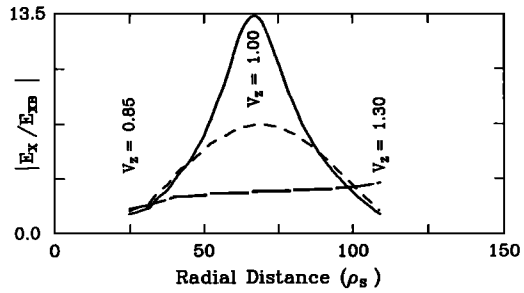

Figure 4. The amplitude of the maximum of E_x, normalized to the boundary value E_{xb}, versus the position of the resonance inside the inhomogeneous region for three different ratios of the length of the inhomogeneous region to the total size of the computational domain: long-dashed line for ratio 1/1.5; short-dashed for the ratio 1/5; and solid line for the ratio 1/10. The normalized phase velocity $v_z = 1$ corresponds in this case to $[(B_1^2 + B_2^2)/(\mu_0(N_1 + N_2))]^{1/2}$ in dimensional variables.

all system length in x that is, respectively, 10, 5, and 1.5 times larger than the width of the density/Alfvén speed ramp. Only the relevant central portion of the total system length in x is shown in the figure.

Except for the case in Figure 4 where the system length is 1.5 times the thickness of the density/Alfvén speed ramp (long-dashed curve), the largest amplitude resonance occurs in the center of the density ramp, at the point where the local Alfvén speed is equal to the phase speed of the surface wave, given approximately as $v_s = [(B_1^2 + B_2^2)/(\mu_0(N_1 + N_2))]^{1/2}$. This value is obtained assuming the thickness of the inhomogeneous region is negligible compared to the perpendicular scale of the surface wave (i.e., the system length when $k_y = 0$) and can be regarded as a limiting case for the present model (see *Chen and Hasegawa* [1974b]; *Hasegawa* [1976]). The long-dashed curve in Figure 4 does not peak in the center because the size of system and the inhomogeneous region are comparable, resulting in a more continuous spectrum of surface waves.

A comparison of the three curves in Figure 4 shows that the effective width of the resonance (full width at half-maximum) decreases as the effective scale size of the Alfvén speed ramp decreases. The variation in peak amplitude for the two curves exhibiting a central peak (solid and short-dashed) is a consequence of the Dirichlet boundary condition on the electric potential. The boundary condition ϕ_b on the electric potential was chosen to be linearly proportional to the system length L_s so that ϕ_b/L_s has the same value for all three cases. We also constructed an analogous figure (not shown) for a Dirichlet boundary condition in which ϕ_b has the same constant value for each case, and we find that the peak amplitude, for cases where there is peak in the center of the layer, is the same for each case, although the full width at half maximum still varies, as shown in Figure 4.

The results shown in Figure 4 suggest to us that, given sufficient time to develop, large-amplitude, dispersive field line resonances are more likely to be found within narrow transverse boundary layers in the density or Alfvén speed. The resonance achieves its largest amplitude in the center of the boundary layer where the coupling between the surface wave and resonant Alfvén wave is strongest. For boundary conditions corresponding to a driven system, the energy deposition in the boundary layer is attributed to large-scale external fluctuations. While the external fluctuations may span a range of frequencies and parallel wavenumbers, the most efficient coupling occurs between external modes with parallel phase speed matching the effective speeds of the surface wave propagating along the boundary layer and the Alfvén speed of the attendant FLR residing within it.

The efficiency of coupling between the boundary driver (representing the external fluctuation), the surface wave at the density ramp, and dispersive resonant Alfvén waves decreases significantly when $k_y L_s > 1$. Figure 5 shows the maximum amplitude of E_x, again calculated from (7), as a function of k_y with v_z fixed at 1. Two effects cause the amplitude to decrease with increasing k_y. As noted above, the amplitude of the surface wave at the density transition decreases exponentially in the homogeneous regions with an e folding length of k_y^{-1}. In addition, a surface wave is also attached to the right boundary (the location of the driver) with amplitude decreasing as $\exp(k_y(x - x_b))$ where x_b is the value of x at the right boundary. This boundary surface wave is an artifact of placing a computational boundary in what is otherwise a continuous portion of the magnetosphere. The overlap between the two exponentially decreasing surface waves is small when the distance between the center of the density ramp and the right boundary exceeds $2/k_y$. Consequently, it becomes increasingly difficult to couple energy contained in the boundary oscillation into the resonance layer at larger values of k_y.

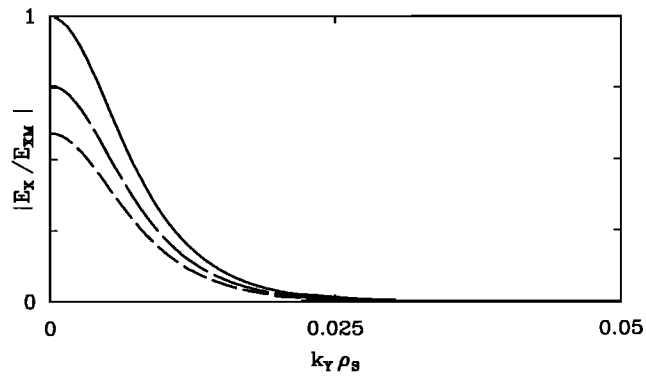

Figure 5. The amplitude of the maximum of E_x in the resonance layer, normalized to the maximum value E_{xm} at $k_y = 0$, versus $k_y\rho_s$. Full solution (solid line) corresponds to solution in the upper panel of Figure 3; the low-frequency portion of the solution (long-dashed line) corresponds to the thick line in the lower panel of Figure 3; and the high-frequency portion of the solution (short-dashed line) corresponds to the thin line in the lower panel of Figure 3.

FLR stimulation by an external driver may actually be less efficient in the small k_y limit than the results in Figure 5 suggest. In the classical (one-fluid MHD) model, energy is tunneled to the resonance by the compressional fast mode. However, excitation by a compressional driver becomes increasingly inefficient as $k_y \to 0$ because the compressional and shear Alfvén modes are uncoupled at $k_y = 0$. Maximum coupling occurs at $k_y \simeq 0.5(k_\parallel^2 v_A^2 dv_A^{-2}/dx)^{1/3}$ for a linear density profile [*Kivelson and Southwood*, 1986]. For the numerical parameters of Figure 5, this estimate gives $k_y\rho_s \approx 0.023\beta_e^{1/3} \approx 0.01$ (taking $\beta_e \approx 0.1$). If we were to assume that maximum coupling efficiency occurs at this value, then Figure 5 suggests that the amplitude at maximum efficiency (i.e., at $k_y\rho_s = 0.01$) is only about 10% of the value at $k_y = 0$. However, the "classical" estimate for k_y at maximum coupling does not include the possible influence of an MHD surface wave at a density boundary layer. The field of the surface wave extends the influence of the resonance out to a distance of at least k_y^{-1} beyond the resonance point, so the coupling efficiency may be considerably larger if a density boundary layer is located near the fast mode cutoff, that is, a boundary layer superimposed on a more gradual perpendicular gradient in Alfvén speed. In addition, large-scale dispersive effects arising from the curvature of the geomagnetic field, combined with the finite plasma pressure, can significantly enhance energy transport to the resonance (over the "classical" estimate) owing to a dispersive propagation band attached to the low Alfvén speed side of the resonance [*Kouznetsov and Lotko*, 1994]. A quantitative assessment of the coupling to the compressional mode requires a fully compressible two-fluid treatment. We emphasize that the (isotropic) compressional mode cannot be treated here because it is eliminated from the reduced two-fluid model by the high-aspect ratio approximation.

In considering the relationship between resonant Alfvén waves and auroral structure, the above analysis suggests at least three reasons to concentrate efforts on the shear Alfvén wave in the small k_y limit ($k_y v_D \ll k_\parallel v_A$) and thereby ignore its coupling to the drift wave: (1) Observations of auroral arcs, which extend coherently over large distances in local time while remaining narrowly confined in latitude, indicate that k_y is very small compared with k_x in these structures. (2) The results in Figure 5 indicate that the level of saturation for drift-Alfvén waves driven by external fluctuations is much lower than for a resonant Alfvén wave; in fact, for the parameters of Figure 5, the drift wave couples to the kinetic Alfvén wave only when $k_y\rho_s \approx 10$, at which point it becomes practically impossible to tap the reservoir of energy contained in external fluctuations in the magnetotail or magnetospheric boundary regions. (3) Even in the resonance region, where locally $k_x = 0$, the drift-Alfvén wave preserves its kinetic property (finite $k_\perp$ and corresponding parallel electric field) which means that the drift-Alfvén wave should be more strongly affected by both electron and ion Landau damping [*Hasegawa*, 1976]. In the next sections we will consider only the case $k_y = 0$. It is clear from (5)–(7) that the ion pressure does not influence the resonance for this case.

2.3. FLR With Parallel Inhomogeneity

Now suppose the plasma is inhomogeneous along the ambient magnetic field as well as perpendicular to it. The associated parallel variation in the Alfvén speed introduces a transition from positive to negative dispersion in the Alfvén wave at some point along the field line.

Because $\mathbf{B}_0$ is taken to be constant, a parallel variation in the background Alfvén speed will be modeled via a parallel density gradient. This assumption, together with our use of an isothermal electron equation of state (constant T_e), implies a nonzero parallel gradient in the background electron pressure. A parallel electron pressure gradient requires, in equilibrium, either a parallel electric field or a parallel gradient in the electron parallel velocity. However, the equations we have been working with implicitly assume that all background parallel gradients are zero. At this point, we therefore abandon the self-consistency of the full three-dimensional, nonlinear two-fluid equations given at the beginning of section 2 in the interest of modeling, more realistically, Alfvén wave propagation characteristics in a more limited two-dimensional, linear model based on a simple uniform background magnetic field.

The parallel gradient in the Alfvén speed that points from the equator toward the ionosphere along auroral field lines will be modeled by a gradient in N_b that points in the opposite direction. As can be seen from the dispersion relation following (11), below, a decreasing N_b produces an increasing Alfvén speed in the dispersion relation (coefficient of k_z^2 when N_b is factored out of the denominator) and an increase in the coefficient δ/N_b of the inertial dispersion term in the denominator. The fact that a qualitatively correct variation in these coefficients is accomplished by a physically incorrect background density profile is not so important in the context of the two-dimensional linear wave equations (1)–(3) with $\partial_y = 0$. However, what is not properly treated here is (1) the actual variation in these coefficients, especially relative to each other, resulting from the actual variation in density and magnetic field intensity, and (2) the parallel variation of the kinetic dispersion term represented by k_x^2 in the numerator of the dispersion relation. Realistically, the influence of the kinetic dispersion term becomes negligible at low altitude where $v_A \gg v_{Te}$. In dimensional variables the coefficient of this term is proportional to ρ_s^2 and, therefore, to T_e/B_0^2. If we were to insist on a self-consistent equilibrium of the reduced two-fluid equations, while allowing a magnetospheric-directed gradient in N_b, then $\partial_z P_{eb} = 0$ would require an ionospheric-directed gradient in T_e. With uniform B_0, this gradient in T_e would incorrectly augment the influence of the kinetic dispersion at low altitude relative to its influence at high altitude. It is clear that holding T_e constant works better (however imperfectly) for the two-dimensional linear

wave model with uniform magnetic field than trying to maintain self-consistency with a zero pressure gradient condition.

A self-consistent model, including realistic parallel variations in density, temperature, and magnetic field strength, can be accomplished by solving the reduced two-fluid equations in dipole magnetic geometry. The less realistic, but also much simpler, model used here turns out to be adequate for illustrating some of the basic features of resonant dispersive Alfvén waves on auroral field lines.

For two-dimensional perturbations, with $\partial_y = 0$, the linear wave equations (1)–(3) become

$$N_b \frac{\partial}{\partial t} A - \delta \frac{\partial}{\partial t} A_{xx} = \frac{\partial}{\partial z} N_d - N_b \frac{\partial}{\partial z} \Phi \tag{9}$$

$$\frac{\partial}{\partial t} N_d = -\frac{\partial}{\partial z} A_{xx} \tag{10}$$

$$\frac{\partial}{\partial t} \left(\frac{\partial}{\partial x} \left(N_b \frac{\partial}{\partial x} \Phi \right) \right) = -\frac{\partial}{\partial z} A_{xx} \tag{11}$$

When the inhomogeneity is weak, so that the variation with x and z occurs parametrically through $N_b(x, z)$, the dispersion relation for (9)–(11) is

$$\omega^2 = k_z^2 \frac{1 + k_x^2}{N_b + \delta k_x^2}$$

Using the notation $\bar{\delta} = \delta / N_b$, the components of the group velocity can be given as

$$v_{gz} = \left(\frac{1 + k_x^2}{1 + \bar{\delta} k_x^2} \right)^{\frac{1}{2}} N_b^{-\frac{1}{2}} \tag{12}$$

$$v_{gx} = k_x k_z \left(\frac{1 + \bar{\delta} k_x^2}{1 + k_x^2} \right)^{\frac{1}{2}} \frac{1 - \bar{\delta}}{(1 + \bar{\delta} k_x^2)^2} N_b^{-\frac{1}{2}} \tag{13}$$

It can be seen from (13) that the perpendicular component of the group velocity changes sign at the point where $\bar{\delta} = 1$. In physical variables this is the point along the magnetic field line where $v_A = v_{Te}$. As noted in section 2.1, the dispersion is positive at altitudes above this point (due to finite thermal effects) and negative below it (due to electron inertia). As a result of the change in direction of the perpendicular group propagation, a dispersive Alfvén wave that initially propagates Earthward, say (toward lower L–shells), above the transition point where $\bar{\delta} = 1$, will turn and propagate tailward (toward higher L–shells) below it. After reflection from the ionosphere, the wave changes its parallel direction of propagation, without changing its perpendicular group velocity until it again passes through the dispersion layer where $\bar{\delta} = 1$. To the extent that the propagation of a dispersive Alfvén wave follows a ray path (a concept that is not likely to be valid for fundamental mode and low harmonic resonances), the whole pattern of the ray trajectory resembles a figure "8," which may not necessarily form completely closed loops (compare Figure 6).

The above considerations are mostly qualitative because expressions (12) and (13) were obtained under the assumption of constant wave amplitude (geometrical optics). In order to develop a more quantitative understanding of the propagation of the dispersive Alfvén waves through an inhomogeneous plasma, we have performed two-dimensional numerical simulations.

3. Numerical Simulations

The simulation box can be considered as a straightened-out auroral flux tube with conducting ionospheres bounding the top and bottom of the simulation domain. The effects of the conducting ionosphere will be modeled primarily through boundary conditions on the two-fluid equations. In simplest form, the ionospheric boundary can be treated as a perfect conductor on which the tangential electric field must vanish: the so-called "short circuit" boundary condition discussed by *Mallinckrodt and Carlson* [1978].

A transverse variation in the Alfvén speed is positioned in the central portion of the simulation box, increasing to the right, as shown in Figure 2. For applications to flux tubes connecting the ionospheres to the near-Earth, equatorial plasma sheet, this gradient, if it were to span the entire width of the simulation box, could represent the gradual Earthward directed gradient in Alfvén speed that arises primarily due to the increase in magnetic field with decreasing radial distance [e.g., *Moore et al.*, 1987]. In this case, however, the gradient scale length is comparable to the system length and, based on the results shown in Figure 4, the resulting resonances may be comparatively weak. The gradient in density (and Alfvén speed) can be steeper and more localized on flux tubes threading the outer ring current/near-Earth plasma sheet, where larger amplitude resonances may occur due to the enhanced coupling to external fluctuations provided by the MHD surface wave. The numerical results described below are appropriate for the latter configuration. A magnetic field–aligned gradient in the Alfvén speed, pointing symmetrically from the equatorial plane to both ionospheres, as discussed in the previous section, is also introduced.

Along the resonance line the background Alfvén speed varies from 1 at the middle of the computational domain to 2.2 near the ionospheres. In the radial direction in the equatorial plane, the background Alfvén speed changes by a factor of about 1.7 through the boundary layer, as shown in Figure 2. While the perpendicular variation in density and Alfvén speed used in the simulations can be justified by appealing to observations (see section 4.2), the parallel variation in the Alfvén speed is much weaker than the nominal variation shown in Figure 1. Nevertheless, this relatively weak parallel variation does introduce a sign change in the dispersion of the Alfvén wave (i.e., there is point along the magnetic field where $v_A = v_{Te}$). The effects of this transition are now considered.

A fourth-order predictor-corrector method is used to time-advance the linear wave equations (9)–(11). The Adams-Bashforth Four-Step Method is used as a predictor and the Adams-Moulton Three-Step Method as a corrector. A disadvantage of this approach is its large memory requirement compared with a Runge-Kutta method of the same order, but this method is much more efficient in terms of the number of computations because one only need calculate the values on the right-hand sides of the system of equations once per time step.

An oscillating boundary condition (Dirichlet on the electric potential function) is imposed on the right boundary. The boundary oscillation frequency and mode number k_z have been chosen to excite a monochromatic MHD surface wave inside the box with $k_y = 0$. This wave couples to a resonant shear Alfvén mode at the critical point (actually a field line extending between the two ionospheres) where the local Alfvén speed is equal to the phase velocity of the surface wave. Initially the resonant oscillation develops a Gaussian-like profile in E_x or B_y centered on the critical line. This is the sort of profile one would obtain from a compressible one-fluid MHD model during the initial phase of evolution of the resonance before other effects become important. As time proceeds, the effective perpendicular scale size of the resonant oscillation decreases until dispersion becomes important. The resonance then begins to radiate dispersive Alfvén waves which propagate energy away from the resonance layer in the perpendicular directions [*Inhester*, 1987; *Wei et al.*, 1994]. The electric and magnetic potentials are held at zero on the left boundary.

We now wish to examine the influence of the parameter $\delta = (v_A/v_{Te})^2$ specified, say, at the equator. The field-aligned variation in $(v_A/v_{Te})^2$ with altitude is determined entirely by the parallel density profile in the simulations because both the background magnetic field and electron temperature are taken to be constant. Therefore, depending on the local value of $\bar{\delta} = \delta/N_b(x,z)$, which determines the sign of the group velocity in (13), the dispersive Alfvén wave will propagate to the left or to the right. For the profiles of v_A and v_{Te} shown in Figure 1, $v_A = v_{Te}$ approximately halfway between the equator and the ionosphere. For the parallel density and Alfvén speed profiles used in the computer simulation, the transition point occurs halfway between the ionosphere and equator when $\delta \approx 0.55$ (equatorial value). We performed three computations, each with a different value of δ but with the same density profile, $N_b(x,z)$, so that the location of the transition point is determined by the value of δ. (Note that $\bar{\delta} = \delta$ by design at the equatorial midpoint.) The three values represent cases where the transition point is near the halfway point ($\delta = 0.555$), closer to the ionosphere ($\delta = 0.450$), and closer to the equator ($\delta = 0.650$).

In all three cases mode 6 (i.e. six half wavelengths between ionospheres) is excited by the driver on the right boundary with oscillation frequency equal to 0.1 ω_{ci}. Our choice of mode 6 is somewhat arbitrary. We have chosen a relatively high mode number at this point so that the simulation results can be compared with physical insights derived from WKB concepts and the linear dispersion relation. The variation in the results described below, for different mode numbers, is left for a future study.

The main results of the simulations are shown in Plate 1. The left frame shows the amplitude of the perpendicular electric field E_x at time 10,950 ω_{ci}^{-1} when $\delta = 0.450$. Because the transition points are closer to the ionospheres for this case, the wave spends more time in the kinetic regime between the transition points than in the inertial regime between them and the ionospheric boundaries. After many reflections of the dispersive Alfvén waves off the two ionospheres (at top and bottom), the pattern resembles a standing Alfvén wave (the resonance), radiating kinetic Alfvén waves to the left. Superficially this pattern resembles the one shown in Figure 3. The right frame in Plate 1 shows the amplitude of E_x at time 4,500 ω_{ci}^{-1} when $\delta = 0.650$. Now the transition points are closer to the equator so the wave spends more time in the inertial regime, and the pattern appears to be radiating inertial Alfvén waves to the right. Recall that the Airy pattern for an inertial Alfvén wave faces on the opposite side of the resonance from a kinetic Alfvén wave.

The middle frame in Plate 1 ($\delta = 0.555$) shows the case where the radiated, dispersive wave dwells in the inertial and kinetic regimes in nearly equal measure in its roundtrip traversal between ionospheres. In effect, refraction to the left by positive dispersion between the two transition points (where $\bar{\delta} = 1$) is exactly compensated by refraction to the right by negative dispersion between the two transition points and the ionospheres. The energy that concentrates in the resonance cannot be radiated away in this case and remains confined to the neighborhood of the resonance point.

Qualitative ray paths for the three different cases are illustrated in Figure 6. The left, middle, and right panels represent parameter regimes similar to those considered in the corresponding panels in Plate 1. The middle panel in Figure 6 shows a ray path closing on itself, forming a figure "8" pattern between ionospheres. The overall propagation to the left and right is perfectly balanced for this case. (For simplicity, only the refraction at the two transition points is indicated in the figure.) In the left panel the transition points are closer to the ionospheres so the wave travels to the left in the kinetic dispersion regime more than it travels to the right in the inertial dispersion region. Consequently, the dispersive Alfvén wave acquires a net propagation to the left. The latter situation is reversed in the right panel where the dispersion transition points are closer to the equator than in the middle panel.

The time evolution of the maximum amplitude of E_x and B_y for each case in Plate 1 is plotted in Figure 7. The common feature of the three runs is the apparent increase in amplitude once the boundary driver is switched on, followed by an eventual saturation. Saturation in these simulations can be attributed to two

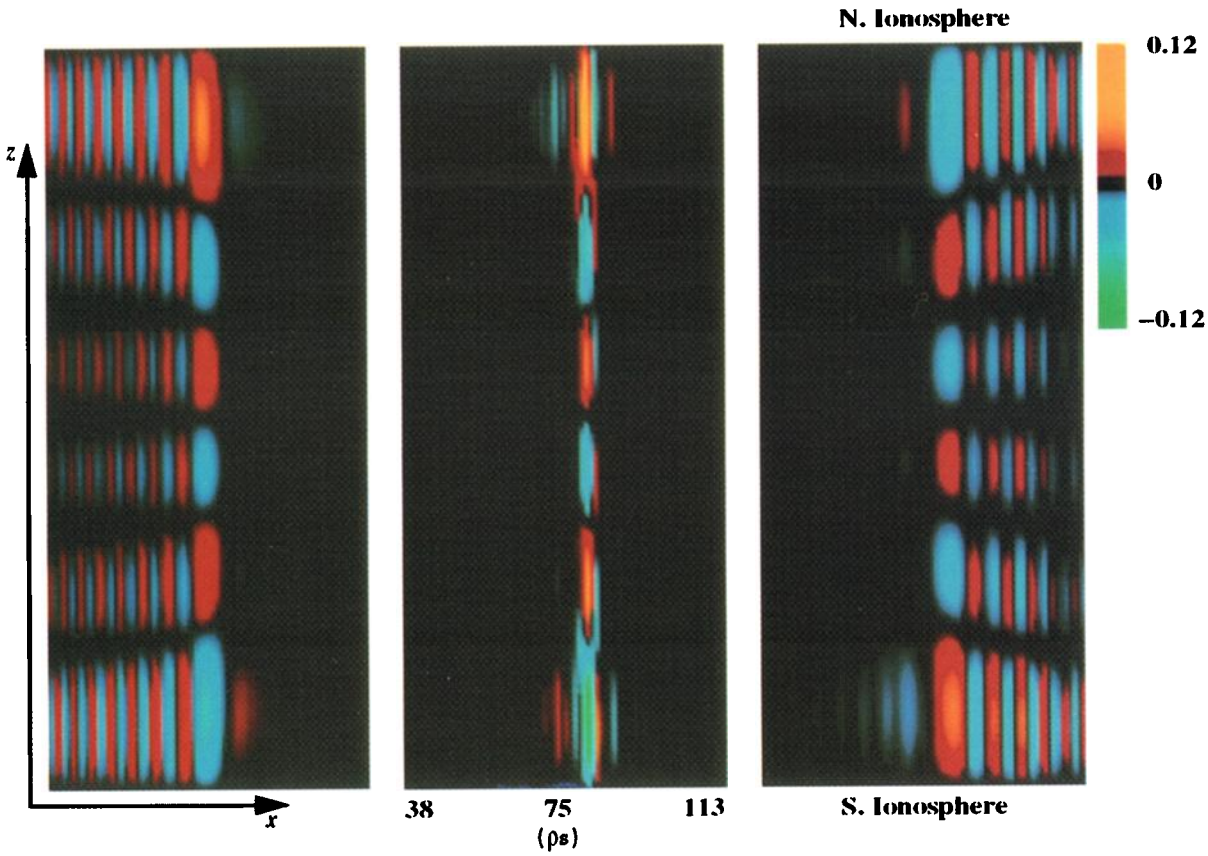

Plate 1. Two-dimensional snapshots of the distribution of E_x in the computational domain for three different values of δ. (left panel) $\delta = 0.450$ at time 10,950 ω_{ci}^{-1}. (middle panel) $\delta = 0.555$ at 11,250 ω_{ci}^{-1}. (right panel) $\delta = 0.650$ at 4,500 ω_{ci}^{-1}. The perpendicular size of the box and the perpendicular background inhomogeneity are the same as in Figure 2. The parameters of the boundary oscillation stimulate a resonance at $x = 75\rho_s$, corresponding to $v_z = v_A = 1$ in Figure 2.

processes: (1) radiation of energy away from the resonance by dispersive Alfvén waves and (2) numerical dissipation due to the finite-difference scheme. There is no dissipation in these runs at the perfectly conducting ionospheric boundaries. Nonlinear spectral transfer cannot take place in the linearized equations (9)–(11) that are solved. Although nonphysical numerical dissipation is present, the difference in saturation amplitude evident in Figure 7 between the middle case ($\delta = 0.555$) and the other two is physically significant. The saturation amplitude for $\delta = 0.555$ is about 2.5 times larger than that for the other two cases which are nearly equal. Energy in the resonance for $\delta = 0.555$ cannot escape by radiating dispersive Alfvén waves because the ray paths, as noted above, close on themselves. For this case, the saturation amplitude is limited by numerical dissipation. On the other hand, saturation for $\delta = 0.450, 0.650$ is largely achieved once the energy supplied to the resonance by the surface wave is balanced by losses due to radiated, dispersive Alfvén waves. For all three cases the amplitude of the saturated electric field in the resonance layer is at least two orders of magnitude larger than the electric field amplitude near the boundary.

When parallel inhomogeneity is neglected, *Inhester* [1987] estimates that the resonance begins radiating dispersive Alfvén waves at time $t_d \approx 0.2/(k_\parallel \rho_s dv_A/dx)$. For the equatorial magnetospheric parameters used in Plate 1, this formula gives a dispersion time for mode 6 of $t_d \approx 200\omega_{ci}^{-1}$. In the upper and lower panels in Figure 7, where saturation is attributed to radiation of dispersive Alfvén waves, the amplitude begins to saturate at about $2000\omega_{ci}^{-1}$. This time is clearly much longer than the predicted dispersion time, indicating that the dwell time of the radiated Alfvén waves in the vicinity of the resonance is much greater when the effects of parallel inhomogeneity are included. The increased dwell time is primarily a geometrical effect, as illustrated in Figure 6.

The wave electric field intensities shown in Plate 1 are in all cases largest near the ionospheric boundaries. (Of course, the boundary conditions require $E_x = 0$ exactly at these boundaries.) This effect is a consequence of the dispersive property of the Alfvén wave combined with WKB-like focusing of the wave intensity where the group speed is large. While this intensification is clearly noticeable in Figure 6, it is relatively weak compared to what is actually expected on auroral field lines. As noted above, the Alfvén speed in the computations varies by a factor of only 2.2 between the equator and the ionospheres whereas this variation is

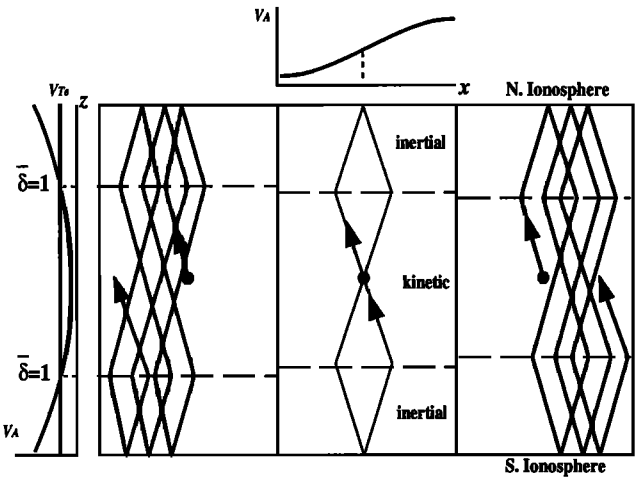

Figure 6. Schematic plot of the ray trajectories for mode 6 when the ray paths form closed loops. The arrows indicate the direction of propagation of a dispersive Alfvén wave. The left, right, and middle panels represent parameter regimes similar to the corresponding panels in Plate 1.

closer to a factor of 50 in Figure 1. The intensification of the wave electric field at low altitude in a dispersive FLR, for more realistic Alfvén speed variations, will be examined in detail in a subsequent manuscript.

4. Discussion

4.1. Model Applicability

The physical approximations introduced at the beginning of section 2 limit applications of the above results to small-amplitude, low-frequency ($\omega \ll \omega_{ci}$), magnetically incompressible fluctuations in a low-β plasma, in which the sound Mach number of the perturbed flow remains small. The perpendicular scale size of the fluctuations must be much larger than the ion Larmor radius but small compared with the parallel scale size of the fluctuations. On a given flux tube, the ion Larmor radius and plasma β are largest near its equatorial crossing point where the ion gyrofrequency is smallest. These approximations therefore apply to fluctuations whose equatorial magnetospheric (outer ring current/near-Earth plasma sheet) signatures exceed about 100 km in the radial direction and vary on timescales exceeding a few seconds.

In the near-Earth plasma sheet, the plasma β can exceed 1 where the plasma pressure is dominated by the energetic and very tenuous ring current or partial ring current particles. These energetic particles have little influence on the wave propagation characteristics considered here, which are determined largely by the bulk plasma characteristics. Bulk plasma measurements from the AMPTE/IRM satellite, spanning energies from 10 eV up to tens of keV, indicate that the plasma β calculated for this range of energies is usually of the order of 0.1 in this region. The low sound Mach number condition is satisfied for equatorial magnetospheric electric fields of the order of a few millivolts per meter or smaller. Radial electric fields of this magnitude, with a radial scale length of 100 km or greater, project geometrically along magnetic field lines to low altitude (say 1000 km) to a north-south field value of the order of 100 mV/m or smaller at 3 km north-south scales or larger. These approximations, including incompressibility ($\delta n/n \ll 1$), are realized for a wide class of electromagnetic disturbances observed at auroral latitudes, including low-frequency electromagnetic fields associated with kilometer-scale auroral arcs.

The idealizations of the magnetospheric-ionospheric system that have been introduced to simplify the mathematical and numerical analysis are more limiting than the above physical approximations. At this point in the development of the model, the ionospheres are treated as perfectly conducting boundaries located at the peaks in Alfvén speed that occur at about 1 R_E altitude in Figure 1. Consequently, detailed characteristics of the model electromagnetic fields cannot be compared di-

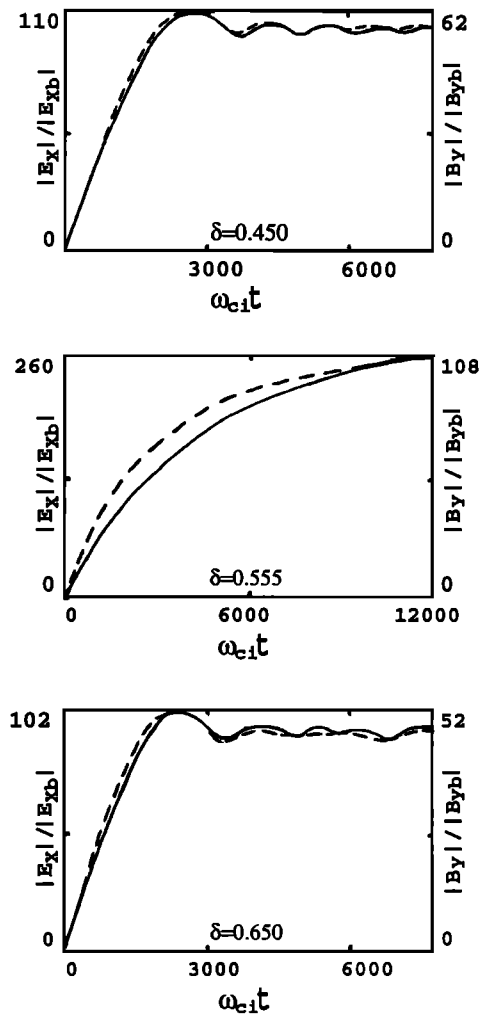

Figure 7. Time evolution of the maximum amplitudes of E_x/E_{xb} (solid line) and B_y/B_{yb} (dashed line) in the computational domain for $\delta = 0.450$ (upper panel), $\delta = 0.555$ (middle panel), and $\delta = 0.650$ (lower panel). E_{xb} and B_{yb} are the (arbitrary) boundary values of E_x and B_y.

rectly with low-altitude satellite or rocket data. Because the background magnetic field is taken to be uniform, it was necessary to introduce a parallel gradient in the background density to model the parallel variation in Alfvén speed. Furthermore, the model gradient in v_A produced by this density gradient is at least a factor of 10 weaker than the nominal parallel gradient in v_A resulting from the variation in dipole field strength. Therefore the period of standing Alfvén waves and their parallel mode structure are not well modeled here, and the effect of positive dispersion (due to the finite electron temperature) on the wave refraction is probably enhanced relative to the actual situation.

4.2. Rugged Properties of Dispersive FLRs

Despite the various approximations and simplifications of the model, dispersive field line resonances do exhibit a number of rugged properties that are retained in a simple model and that can be compared in a qualitative way with various observations.

Resonant surface. Our results indicate that large-amplitude resonances are likely to be found at abrupt transitions in the Alfvén speed (perpendicular gradient scale length in v_A << typical azimuthal wave length of the FLR). What evidence exists for small-scale density transitions in the nightside magnetosphere, of the type shown in Figure 2, that may be superimposed on the large-scale, Earthward directed gradient in the Alfvén speed? We mention first that the edges of the so-called auroral plasma cavity, observed at altitudes of about 2000 km up to $3R_E$ or more [*Persoon et al.*, 1988], exhibit steep density changes up to a factor of 10 or greater. Furthermore, the S3-3 electric field experiment [*Mozer*, 1980] has shown that large-amplitude electric fields resembling those in field line resonances usually occur at the edges of the auroral acceleration region, which coincides with the auroral plasma cavity. Several rocket experiments have also shown that large-amplitude, small-scale Alfvén waves, intense electron fluxes, and discrete auroral arcs are observed at the poleward and equatorward edges of inverted-V precipitation regions [*Boehm et al.*, 1990; *Timofeev and Galperin*, 1991; *Earle and Kelly*, 1993; *Torbert et al.*, 1994]. Since inverted-V precipitation is essentially the low-altitude signature of the large-scale (~ 100 km transverse), quasi-static, parallel electric field that evacuates the auroral plasma cavity, it seems safe to assume that the edge-region Alfvén waves observed at rocket altitudes are the lower altitude signature of concentrated resonant Alfvén waves standing along the steep density gradients of the auroral plasma cavity.

Observations of steep, localized density gradients in the outer ring current/near-earth plasma sheet region are not as well documented. *McIlwain* [1980] has suggested that cold plasma boundaries (density gradients) are left more or less intact in this region following "substorm injections." The boundary layers presumably persist on a diffusive timescale during quiescent periods but may be later swept away during a subsequent substorm. One reported density profile derived from

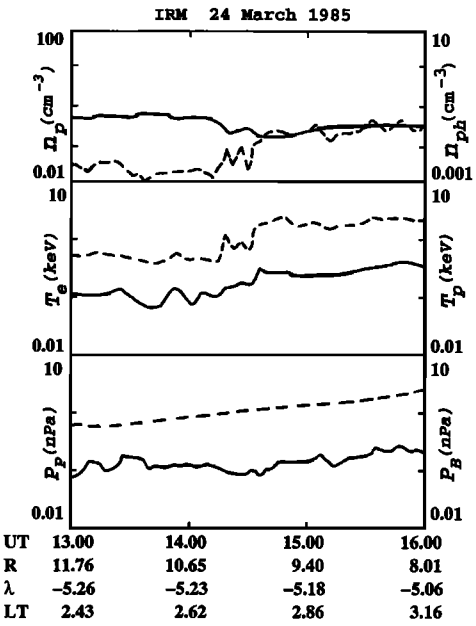

Figure 8. An AMPTE/IRM observation on March 24, 1985, of density boundary layers near the inner edge of the plasma sheet. At least two steps in the bulk plasma density (n_p), each approximately a factor of 4 change, are evident at about 1415 and 1430 UT. The boundary layers occur in a region where the hot proton density (n_{ph}) undergoes a larger-scale Earthward increase of about a factor of 10 while the bulk electron (T_e) and proton (T_p) thermal energies increase overall by a factor of about 5. The change in density through the boundary layer is inversely proportional to the change in thermal energy so that the total plasma pressure (P_P) is nearly constant through the layer. The magnetic pressure (P_B) exhibits a large-scale, Earthward increase. Notice that $\beta \leq 0.1$ from 1400 UT onward. The satellite coordinates R, λ, and LT represent geocentric radial distance, magnetic latitude, and local time.

the ISEE 1 plasma wave experiment shows fairly convincing evidence for several density boundary layers between L=6 and 9 near the inner edge of the postmidnight plasma sheet. Although *Hughes and Grard* [1984] compiled this density profile primarily for purposes of estimating the field line eigenperiods, we point out here that the amplitude of the toroidal component of the second harmonic resonances studied by them shows some tendency to peak within or near the inferred boundary layers.

We have also searched for evidence of density boundary layers in the AMPTE/IRM data set when the satellite was traversing, primarily radially, the region from 8-12 R_E, near the equatorial plane, and within a few hours of local midnight. Our survey was fairly limited, but we did find a number of relatively sharp density transitions similar to those modeled in this paper. The observed transitions may be quasi-stationary, although it is difficult to distinguish between a static and traveling pattern based on data from a single satellite. One of the more striking events is shown in Figure 8. Note the two density steps at about 1415 and 1430 UT. The

density changes by a factor of 4 over a distance less than about 1000 km if the temporal variation is interpreted entirely as satellite motion through a spatial structure. The thermal plasma β is about 0.1 throughout the region, and the perpendicular scale length for variation in the plasma and magnetic pressures is much greater than that of the density steps. (Overall pressure balance clearly forces the plasma temperature to vary inversely with the density.) We show this figure here simply to demonstrate the existence of transitions in density in the near-Earth plasma sheet that are similar in form to those considered in this paper. Although the associated gradient in the Alfvén speed is directed earthward for the tailward directed density gradient in Figure 8, relatively steep density gradients pointing in the opposite direction can also be found (and are also present in the above cited work by Hughes and Grard).

Mode selection. Given that an external driver tends to couple strongly to a dispersive field line resonance (1) at steep density gradients in the magnetosphere, (2) when the mode structure and frequency of the driver match those of a surface wave propagating along the density boundary layer, and (3) when the azimuthal (or cross-tail) wavelength of the driver is large, the criteria for FLR mode selection become fairly restrictive. If the spectrum of the external driver is broad, only those modes with frequencies matching the resonant eigenfrequencies (fundamental and harmonics) near the center of the boundary layer efficiently couple energy into the dominant field line resonance. We emphasize, however, our study has been limited to parallel eigenmode 6. Additional selection criteria may favor either the fundamental or various harmonics of the resonance. Condition (3) tends to produce resonant structures with ionospheric signatures that are elongated in magnetic local time and narrow in latitude. These long, narrow structures are reminiscent of the discrete auroral arcs that occur near the edges of inverted-V precipitation regions.

Strongly radiating FLRs. The radiation of obliquely propagating, dispersive Alfvén waves by a field line resonance can be a major factor limiting the amplitude of the resonance. How strongly the FLR radiates dispersive Alfvén waves depends, in turn, on the background variation in the Alfvén speed, both parallel and perpendicular to the ambient magnetic field. In contrast with their weakly radiating counterparts, strongly radiating FLRs tend to be broader in the transverse direction owing to their Airy-like oscillatory patterns. The decaying oscillation can face either equatorward or poleward depending on the direction of the transverse gradient in the Alfvén speed and its parallel profile, which determines whether kinetic or inertial dispersion is favored. *Torbert and Mozer* [1978] show a nice example from the S3-3 satellite data of decaying oscillations in the electric field measured near the edges of an inverted-V precipitation region that seems to fit the radiating FLR scenario very well (see their Figure 1).

Weakly radiating FLRs. Under special circumstances, the tendency of the FLR to radiate may be compensated by refraction, leading to dispersive Alfvén ray paths that circulate on closed, or nearly closed, trajectories around the FLR. For such events, the amplitude of the nonradiating FLR must be limited by some other process (e.g., ionospheric dissipation, wave-particle interactions, nonlinear spectral transfer). The transverse structure of a nonradiating FLR tends to be more localized than its radiating counterpart, and its amplitude exceeds that of a radiating FLR, all other conditions being equal. Some of the so-called S and V electrostatic shocks of the S3-3 data set [*Mozer*, 1980; *Temerin et al.*, 1981a, b] are prime candidates for nonradiating or weakly radiating FLRs (if we may be permitted to revise the early nomenclature used to describe some of the large-amplitude electric fields in the S3-3 data), as are the so-called solitary kinetic Alfvén waves observed on Freja [*Louran et al.*, 1994], the large-amplitude electric fields observed on DE-1 [*Weimer and Gurnett*, 1993], and the electromagnetic disturbances observed on ICB-1300 that *Dubinin et al.* [1990] have convincingly shown to be standing Alfvén waves. The main point to be noted here is that observed FLR structures that are more localized tend have larger amplitudes, in a statistical sense, than the broader and more oscillatory FLR structures. This statistical trend seems to be present in the observations.

It is not obvious, however, that the simple FLR model developed here can explain why large-amplitude electric fields at the edges of 100 km scale transverse, auroral acceleration regions, that is, the high-altitude extension of inverted-V precipitation regions, are usually (though not always) polarized as if the structure were electrostatic, with the perpendicular E field pointing toward the center of the structure [*Temerin et al.*, 1981a]. If these fields are simple FLRs, one would expect the polarity of the observed electric field to reverse periodically in time due to the oscillatory nature of the attendant standing Alfvén waves. Perhaps FLRs coexist, or are even promoted by inverted-V, edge region electrostatic fields. The events reported by *Temerin et al.* [1981a] certainly show cases where an oscillatory pattern is superimposed on a seemingly electrostatically polarized, edge region electric field.

Intensification at low altitude. The electromagnetic energy flux in a dispersive FLR tends to concentrate in the lower altitude portion of the flux tube, at some distance above the ionosphere where the boundary conditions ultimately force the electric field to be zero. Furthermore, there are indications in our work that dispersive effects are not always sufficient to limit the secular temporal growth of the resonance, in particular, when the resonance is nonradiating. In such cases the intensification at low altitude may be especially large. The degree of intensification is expected to be much greater than is indicated in the simple model considered here, which only yields a factor of about 3 increase in amplitude between the equatorial and low-altitude signatures. To our knowledge, there have been no statistical studies of the distribution of Alfvénic electric fields with altitude. However, studies of large-amplitude elec-

tric fields in the auroral zone that do not distinguish between quasi-static and Alfvénic fields are at least consistent with this behavior [*Weimer and Gurnett*, 1993].

5. Conclusion

Although the theory and phenomenology of field line resonances represent one of the more mature areas of magnetospheric physics, the relationships between the phenomena observed with ground-based instruments, on equatorial magnetospheric satellites, and on low-altitude, polar-orbiting satellites are still not well understood when the resonance width becomes sufficiently small that two-fluid and kinetic effects must be considered. Quantitative models based on realistic magnetic geometry and background density and temperature distributions may provide a useful framework for organizing and connecting relevant data obtained in widely separated regions of the coupled magnetosphere and ionosphere. Our results suggest at least two key areas where further theoretical and observational studies may provide new insights into the phenomena.

One area concerns the phenomenology surrounding plasma density boundary layers in the outer ring current/near-Earth plasma sheet and their relation to auroral structure. How do isolated gradients arise, particularly in the magnetosphere, and what sort of electrical currents, ULF wave activity, and particle signatures accompany the gradients? What are the low-altitude signatures of these isolated gradients?

The second area concerns the refractive properties of dispersive Alfvén waves due to the parallel inhomogeneity of the flux tube. This aspect of Alfvén wave propagation has received very little attention in the literature, and, to our knowledge, this paper represents a first systematic study of some of the consequences of the transition from positive to negative Alfvén wave dispersion that occurs at intermediate altitudes between 4 and 6 R_E. Wave-particle interactions may also be very important in the dispersion transition region, but we are unaware of any literature relevant to the (convective) Landau damping of a dispersive Alfvén wave in a strongly inhomogeneous plasma resembling an auroral flux tube. Unfortunately, this region has also been relatively undersampled by satellites (the early Hawkeye satellite is perhaps an exception), so that the connection between models and observations relevant to this region will probably continue to be based on proxy information obtained at low altitudes and near the equator.

Acknowledgments. We wish to thank C. Carlson, J. Hughes, J. LaBelle, and R. Lysak, as well as referee M. Temerin, for helpful discussions and for comments by G. Paschmann and W. Baumjohann on the AMPTE/IRM data that were conveyed to us. The AMPTE/IRM plasma and magnetic field data have been made available by G. Paschmann and H. Lühr, respectively. The research was supported in part by NASA under grants NAG5-2252, NAG5-1098, and NAGW-3989.

The Editor thanks K. Takahashi and M. A. Temerin for their assistance in evaluating this paper.

References

Allan, W., The ponderomotive force of standing Alfvén waves in a dipolar magnetosphere, *J. Geophys. Res., 98*, 1409, 1993.

Boehm, M. H., C. W. Carlson, J. P. McFadden, J. H. Clemmons, and F. S. Mozer, High-resolution sounding rocket observations of large-amplitude Alfvén waves, *J. Geophys. Res., 95*, 12,157, 1990.

Block, L. P., and C.-G. Falthammar, The role of magnetic-field-aligned electric fields in auroral acceleration, *J. Geophys. Res., 95*, 5877, 1990.

Burke, W. Y., M. S. Gussenhoven, M. C. Kelley, D. A. Hardy, and F. Y. Rich, Electric and magnetic field characteristics of discrete auroral arcs in the polar cap, *J. Geophys. Res., 87*, 2431, 1982.

Chen, L., and A. Hasegawa, A theory of long-period magnetic pulsations, 1, Steady state excitation of field line resonance, *J. Geophys. Res., 79*, 1024, 1974a.

Chen, L., and A. Hasegawa, A theory of long-period magnetic pulsations, 2, Impulse excitation of surface eigenmode, *J. Geophys. Res., 79*, 1033, 1974b.

Chmyrev, V. M., O. A. Pokhotelov, V. A. Marchenko, V. I. Lazarev, A. V. Streltsov, and L. Stenflo, Alfvén vortices and related phenomena in the ionosphere and the magnetosphere, *Phys. Scr., 38*, 841, 1988.

Chmyrev, V. M., V. A. Marchenko, O. A. Pokhotelov, L. Stenflo, P. K. Shukla, and A. V. Streltsov, The development of the discrete active auroral forms, *IEEE Trans. Plasma Sci., 20*, 764, 1992.

Dubinin, E. H., A. S. Volokitin, P. L. Israelevich, and N. S. Nikolaeva, Auroral electromagnetic disturbances at altitudes of 900 km: Alfvén wave turbulence, *Planet. Space Sci., 36*, 949, 1988.

Dubinin, E. M., P. L. Israelevich, and N. S. Nikolaeva, Auroral electromagnetic disturbances at an altitude of 900 km: The relationship between the electric and magnetic field variations, *Planet. Space. Sci., 38*, 97, 1990.

Earle, G. D., and M. C. Kelley, Spectral evidence for stirring scales and two-dimensional turbulence in the auroral ionosphere, J. Geophys. Res., *98*, 11,543, 1993.

Goertz, C. K., Kinetic Alfvén waves on auroral field lines, *Planet. Space Sci., 32*, 1387, 1984.

Goertz, C. K. and R. W. Boswell, Magnetosphere-ionosphere coupling, *J. Geophys. Res., 84*, 7239, 1979.

Gurnett, D. A., R. L. Huff, J. D. Menietti, J. L. Burch, J. D. Winningham, and S. D. Shawhan, Correlated low-frequency electric and magnetic noise along auroral field lines, *J. Geophys. Res., 89*, 8971, 1984.

Haerendel, G., An Alfvén wave model of auroral arcs, in *High-Latitude Space Plasma Physics*, edited. by B. Hultqvist and T. Hagfors, pp. 515-535, Plenum Press, New-York, 1983.

Haerendel, G., S. Buchert, C. La Hoz, B. Raaf, and E. Rieger, On the proper motion of auroral arcs, *J. Geophys. Res., 98*, 6087, 1993.

Hasegawa, A., Particle acceleration by MHD surface wave and formation of aurora, *J. Geophys. Res., 81*, 5083, 1976.

Hazeltine, R. D., and J. D. Meiss, Shear-Alfvén dynamics of toroidally confined plasmas, *Phys. Rep., 121*, 1, 1985.

Hughes, W. J., and R. J. L. Grard, A second harmonic geomagnetic field line resonance at the inner edge of the plasma sheet: GOES 1, ISEE 1, and ISEE 2 observations, *J. Geophys. Res., 89*, 2755, 1984.

Inhester, B., Numerical modeling of hydromagnetic wave coupling in the magnetosphere, *J. Geophys. Res., 92*, 4751, 1987.

Ishii, M., M. Sugiura, T. Iyemori, and J. A. Slavin, Correlation between magnetic and electric field perturbations

in the field-aligned current regions deduced from DE 2 observations, *J. Geophys. Res., 97*, 13,877, 1992.

Kadomtsev, B. B., *Plasma Turbulence*, Academic Press, New York, 1965.

Kivelson, M. G., and D. J. Southwood, Coupling of global magnetospheric MHD eigenmodes to field line resonances, *J. Geophys. Res., 91*, 4345, 1986.

Kletzing, C., C. Cattell, F. S. Mozer, S.-I. Akasofu, and K. Makita, Evidence for electrostatic shocks as the source of discrete auroral arcs, *J. Geophys. Res., 88*, 4105, 1983.

Knudsen, D. J., M. C. Kelley, and J. F. Vickrey, Alfvén waves in the auroral ionosphere: A numerical model compared with measurements, *J. Geophys. Res., 97*, 77, 1992.

Kouznetsov, I., and W. Lotko, Radial energy transport by magnetospheric ULF waves: Effects of magnetic curvature and plasma pressure, *J. Geophys. Res., 100*, 7599, 1995.

Li, X., and M. Temerin, Ponderomotive effects on ion acceleration in the auroral zone, *Geophys. Res. Lett., 20*, 13, 1993.

Louran, P., J. E. Wahlund, T. Chust, H. de Feraudy, A. Roux, B. Holback, P. O. Dovner, A. I. Ericksson, and G. Holmgren, Observations of kinetic Alfvén waves by the Freja satellite, *Geophys. Res. Lett., 21*, 1847, 1994.

Lysak, R. L., Feedback instability of the ionospheric resonant cavity, *J. Geophys. Res., 96*, 1553, 1991.

Lysak, R. L., and C. W. Carlson, Effect of microscopic turbulence on magnetosphere-ionosphere coupling, *Geophys. Res. Lett., 8*, 269, 1981.

Lysak, R. L., and C. T. Dum, Dynamics of magnetosphere ionosphere coupling including turbulent transport, *J. Geophys. Res., 88*, 365, 1983.

Mallinckrodt, A. J., and C. W. Carlson, Relations between transverse electric fields and field-aligned currents, *J. Geophys. Res., 83*, 1426, 1978.

McFadden, J. P., C. W. Carlson, M. H. Boehm, and T. J. Hallinan, Field-aligned electron flux oscillations that produce flickering aurora, *J. Geophys. Res., 92,*, 11,133, 1987.

McIlwain, C. E., Cold plasma boundaries and auroral arcs, in *Physics of Auroral Arc Formation, Geophys. Monogr. Ser.*, vol. 25, edited by S.-I. Akasofu and J. R. Kan, p. 173, AGU, Washington, D. C., 1980.

Moore, T. E., D. L. Gallagher, J. L. Horowitz, and R. H. Comfort, MHD breaking in the outer plasmasphere, *Geophys. Res. Lett., 14*, 1007, 1987.

Mozer, F. S., The low altitude electric field structure of discrete auroral arcs, in *Physics of Auroral Arc Formation, Geophys. Monogr. Ser.*, vol. 25, edited by S.-I. Akasofu and J. R. Kan, p. 136, AGU, Washington, D. C., 1980.

Mozer, F. S., C. W., Carlson, M. K. Hudson, R. B. Torbert, B. Parady, J. Yatteau, and M. C. Kelley, Observations of paired electrostatic shocks in the polar magnetosphere, *Phys. Rev. Lett, 38*, 292, 1977.

Newton, R. S., D. J. Southwood, and W. J. Hughes, Damping of geomagnetic pulsations by the ionosphere, *Planet. Space. Sci., 26*, 201, 1978.

Persoon, A. M., D. A. Gurnett, W. K. Peterson, J. H. Waite, Jr., J. L. Burch, and J. L. Green, Electron density depletions in the nightside auroral zone, *J. Geophys. Res., 93*, 1871, 1988.

Polyakov, S. V. and V. O. Rapoport, Ionospheric Alfvén resonator, *Geomagn. Aeron., 21*, 816, 1981.

Rankin, R., B. G. Harrold, J. C. Samson, and P. Frycz, The nonlinear evolution of field line resonances in the Earth's magnetosphere, *J. Geophys. Res., 98*, 5839, 1993.

Redsun, M. S., M. Temerin, and F. S. Mozer, Classification of auroral electrostatic shocks by their ion and electron associations, *J. Geophys. Res., 90*, 9615, 1985.

Samson, J. C., D. D. Wallis, T. J. Hughes, F. Creutzberg, J. M. Ruohoniemi, and R. A. Greenwald, Substorm intensifications and field line resonance in the nightside magnetosphere, *J. Geophys. Res., 97*, 8495, 1992.

Seyler, C. E., Nonlinear 3-D evolution of bounded kinetic Alfvén waves due to their flow and collisionless tearing instability, *Geophys. Res. Lett., 15*, 756, 1988.

Seyler, C. E., A mathematical model of the structure and evolution of small-scale discrete auroral arcs, *J. Geophys. Res., 95*, 17,199, 1990.

Southwood, D. J., Some features of field line resonances in the magnetosphere, *Planet. Space. Sci., 22*, 483, 1974.

Stix, T. H., *Waves in Plasmas*, chap. 13, Am. Inst. of Phys., New York, 1992.

Streltsov, A. V., Chmyrev, V. M., O. A. Pokhotelov, V. A. Marchenko, and L. Stenflo, The formation and non-linear evolution of the convective cells in the auroral plasma, *Phys. Scr., 41*, 686, 1990.

Temerin, M., M. H. Boehm, and F. S. Mozer, Paired electrostatic shocks, *Geophys. Res. Lett., 8*, 799, 1981a.

Temerin, M., C. Cattell, R. Lysak, M. Hudson, R. B. Torbert, F. S. Mozer, R. D. Sharp, and P. M. Kintner, The small-scale structure of electrostatic shocks, *J. Geophys. Res., 86*, 11,278, 1981b.

Temerin, M., J. McFadden, M. Boehm, C. W. Carlson, and W. Lotko, Production of flickering aurora and field-aligned electron flux by electromagnetic ion cyclotron waves, *J. Geophys. Res., 91*, 5769, 1986.

Timofeev, E. E., and Y. I. Galperin, Convection and currents in stable auroral arcs and inverted-Vs, *J. Geomagn. Geoelectr., 43*, suppl., 259, 1991.

Torbert, R. B., and F. S. Mozer, Electrostatic shocks as the source of discrete auroral arcs, *Geophys. Res. Lett., 5*, 135, 1978.

Torbert, R., et al., Observations of Alfvén waves at the edge of auroral arcs (abstract), *EOS Trans. AGU, 75*, 572, 1994.

Trakhtengertz, V. Y., and A. Y. Feldstein, Turbulent Alfvén boundary layer in the polar ionosphere, 1, Excitation conditions and energetics, *J. Geophys. Res., 96*, 19,363, 1991.

Tsyganenko, N. A., Global quantitative models of the geomagnetic field in the cislunar magnetosphere for different disturbance levels, *Planet. Space Sci., 35*, 1347, 1987.

Xu, B.-L., J. C. Samson, W. W. Liu, F. Creutzberg, and T. J. Hughes, Observations of optical aurora modulated by resonant Alfvén waves, *J. Geophys. Res., 98*, 11,531, 1993.

Walker, A. D. M., J. M. Ruohoniemi, K. B. Baker, R. A. Greenwald, and J. C. Samson, Spatial and temporal behavior of ULF pulsations observed by the Goose Bay HF radar, *J. Geophys. Res., 97*, 12,187, 1992.

Wei, C. Q., J. C. Samson, R. Rankin, and P. Frycz, Electron inertial effects on geomagnetic field line resonances, *J. Geophys. Res., 99*, 11,265, 1994.

Weimer, D. R. and D. A. Gurnett, Large-amplitude auroral electric fields measured with DE-1, *J. Geophys. Res., 98*, 13,557, 1993.

Weimer, D. R., C. K. Goertz, and D. A. Gurnett, Auroral zone electric fields, *J. Geophys. Res., 90*, 7479, 1985.

W. Lotko and A. Streltsov, Thayer School of Engineering, Dartmouth College, 8000 Cummings Hall, Hanover, NH 03755-8000. (e-mail: lotko@dartmouth.edu; streltsov@dartmouth.edu)

(Received January 4, 1995; revised May 15, 1995; accepted May 18, 1995.)